Dynamical Evolution of Quasi-Hierarchical Triples

Yonadav Barry Ginat,[1,2]⋆ Jakob Stegmann[3] and Johan Samsing[4]
[1] Rudolf Peierls Centre for Theoretical Physics, University of Oxford, Parks Road, Oxford, OX1 3PU, United Kingdom
[2] New College, Holywell Street, Oxford, OX1 3BN, United Kingdom
[3] Max-Planck-Institut für Astrophysik, Karl-Schwarzschild-Straße 1, 85748 Garching bei München, Germany
[4] Niels Bohr Institute, Copenhagen University, Blegdamsvej 17, 2100 Copenhagen, Denmark

Accepted XXX. Received YYY; in original form ZZZ

ABSTRACT

We study the gravitational dynamics of quasi-hierarchical triple systems, where the outer orbital period is significantly longer than the inner one, but the outer orbit is extremely eccentric, rendering the time at pericentre comparable to the inner period. Such systems are not amenable to the standard techniques of perturbation theory and orbit-averaging. Modelling the evolution of these triples as a sequence of impulses at the outer pericentre, we show, by comparing with direct three-body integrations, that such triples lend themselves to a description as an analytical map between subsequent outer pericentre passages. This map exhibits secular oscillations, going beyond the von Zeipel–Lidov–Kozai mechanism. We show that the time to coalescence due to gravitational waves in such systems is modified. We then study the long-term evolution under this map, which lead to a random-walk-like behaviour of the inner eccentricity. While this behaviour is probably absent from isolated triples, it could exist in triples where the outer orbit is weakly coupled to a system with which it can exchange angular momentum, and we describe some properties of this random walk.

Key words: stars: kinematics and dynamics – gravitational waves – (stars:) binaries (including multiple): close – (transients:) black hole mergers

arXiv:2509.02685v3 [astro-ph.HE] 12 Aug 2026

1 INTRODUCTION

Triple systems are home to an immense range of dynamical and astrophysical phenomena (Valtonen & Karttunen 2006; Perets 2025). They play an important role in the evolution of all many-body astrophysical systems: from planetary systems (Winn & Fabrycky 2015), to massive stars (Offner et al. 2023; Shariat et al. 2025), stellar clusters (Antonini et al. 2016; Martinez et al. 2020; Trani et al. 2022), and galaxies (e.g., van der Marel et al. 2012).

Triple systems of similar component-masses are generally either hierarchical (there is a well-defined inner binary orbited by an outer star, with a clear separation of orbital time-scales) or non-hierarchical (the three stars are in an approximate energy equipartition) and unstable (Perets 2025). Hierarchical triples, which can be stable over long time-scales, can be mathematically treated by means of perturbation theory (e.g., Harrington 1968; Ford et al. 2000; Arnold et al. 2006; Katz et al. 2011; Naoz et al. 2013; Tremaine 2023). Indeed, such systems are usually studied either by direct three-body integrations, or by various analytical techniques, in a hierarchy of approximations (or coarse-graining operations), as one is concerned with the long-term state of the system, rather than the rapid temporal evolution. These include a single orbit-averaging over the inner binary's fast period, where the orbital elements of the inner binary evolve over time-scales comparable to the outer orbit, due to the tertiary's influences, or double orbit-averaging, where the system is averaged over both the inner and the outer orbit (see Naoz 2016; Shevchenko 2017, for reviews). These approximations are adequate when one is concerned with time-scales much longer that the outer period, and in the absence of strong resonances.[1] An example of such a phenomenon is the famous von Zeipel–Lidov–Kozai effect (ZLK; von Zeipel 1910; Lidov 1962; Kozai 1962).

Non-hierarchical, or 'democratic', triples are notoriously chaotic and unstable (Hut 1993; Heinämäki et al. 1999; Mardling & Aarseth 2001; Valtonen & Karttunen 2006; Zhang et al. 2023; Trani et al. 2024b), but ensembles of such systems—as all dense clusters are—may be modelled using statistical theories (Heggie 1975; Monaghan 1976a,b; Valtonen & Karttunen 2006; Stone & Leigh 2019; Ginat & Perets 2021; Kol 2021).

Hierarchical triples, even in the Galactic field, do not exist in isolation: the outer orbit can be wide, and is susceptible to external perturbations, which can affect it significantly (e.g., Michaely & Perets 2019, 2020; Raveh et al. 2022; Grishin & Perets 2022; Stegmann et al. 2024). While triples with an

[1] Note, that this is distinct from a double-averaging procedure of the inner orbit, where the inner pericentre's precession is averaged over—we do not consider such an averaging here.

⋆ E-mail: yb.ginat@physics.ox.ac.uk

© 2026 The Authors

outer semi-major axis of $a_{\rm out} \lesssim \mathcal{O}\left(10^4\right)$ AU are not expected to be disrupted by the Galactic tide (Jiang & Tremaine 2010; El-Badry & Rix 2018); even for outer semi-major axes of order $10^{3\text{–}4}$AU the tertiary may be frequently scattered to a highly eccentric orbit about the inner binary (Stegmann et al. 2024). Thus, the hierarchical triple may enter such a state that the hierarchy of orbital periods is still preserved, but the outer pericentre—while still larger than the inner semi-major axis—is much smaller than the outer semi-major axis. We call such triples *quasi-hierarchical*.

These triples cannot be modelled as regular hierarchical systems, because the time the tertiary spends near pericentre is comparable to (a few times) the inner orbital period. While fully hierarchical systems can be studied perturbatively, and fully democratic ones can be described probabilistically, quasi-hierarchical triples, which inhabit the intermediate range, do not succumb to either treatment: the separation of time-scales is not strong enough for standard triple perturbation theory, but there is still too much structure (not enough phase-space mixing) for a purely statistical-mechanical theory. In terms of eccentricity, we will show below in appendix B that if the outer orbit's eccentricity is $e_{\rm out} \gtrsim 1-\sqrt{a_{\rm in}/a_{\rm out}}$, then the triple becomes quasi-hierarchical. If $e_{\rm out} \gtrsim 1-a_{\rm in}/a_{\rm out}$ the triple becomes unstable (Mardling & Aarseth 2001).

The quasi-hierarchical regime is distinct from other deviations from secularity, where, e.g., double averaging fails because the time-scale separation is not wide enough (Luo et al. 2016; Grishin et al. 2018; Mangipudi et al. 2022). This can be corrected, yielding the Brown Hamiltonian (e.g. Luo et al. 2016; Will 2021; Tremaine 2023; Grishin 2024; Klein & Katz 2024; Lei & Grishin 2025a,b), but these studies still took $e_{\rm out}$ to be moderate, and kept higher-order terms in $\alpha \equiv a_{\rm in}/a_{\rm out}$. The quasi-hierarchical regime here is distinct: the time-scale hierarchy is very wide, but on the other hand $e_{\rm out}$ is very high, too. As perturbers excite $e_{\rm out}$, one thus has three possibilities for the subsequent evolution, summarised in Table 1.

The aim of this paper is to introduce a simple model for the evolution of such a triple, that tracks the inner binary's orbital elements over time. This model will allow us to gauge the time-scale for the evolution of the inner binary's eccentricity (*inter alia*), and hence how fast it reaches values where other effects, such as stellar tidal interactions, stellar collisions, or gravitational-wave emission, become important.

Indeed, since the first direct detection of gravitational waves from a binary-black-hole coalescence by The LIGO Scientific Collaboration et al. (2016), many channels have been proposed for the origin of the binaries seen by the LIGO–Virgo–KAGRA (LVK) collaboration, with the goal of explaining how pairs of compact objects can be brought to tight separations, that allow them to merge within a time shorter than the age of the Universe. These channels include globular or nuclear clusters (e.g., Portegies Zwart & McMillan 2000; O'Leary et al. 2009; Tanikawa 2013; Antonini & Rasio 2016; Rodriguez et al. 2015, 2016; Samsing 2018; Samsing & D'Orazio 2018; Antonini et al. 2025), active galactic nuclei (AGN) (e.g., Bartos et al. 2017; Stone et al. 2017; Trani et al. 2019, 2021, 2024a; McKernan et al. 2020; Tagawa et al. 2020; Samsing et al. 2022, 2024; Rozner & Perets 2022; Grishin et al. 2024; Fabj & Samsing 2024; Whitehead et al. 2024; Gilbaum et al. 2025; Rowan et al. 2025), an isolated channel where the tight binaries are formed via binary stellar evolution (e.g., Belczynski et al. 2002; Dominik et al. 2012; Belczynski et al. 2016; Iorio et al. 2023), and a "triple" channel (e.g., Wen 2003; Antognini et al. 2014; Antonini et al. 2014, 2016, 2017; Rodriguez & Antonini 2018; Fragione & Loeb 2019; Fragione et al. 2019; Bartos et al. 2023; Vigna-Gómez et al. 2025; Stegmann & Klencki 2025), where the black-hole binary is the inner component of a hierarchical triple system, and the tertiary acts as a reservoir with which the inner binary may exchange angular momentum. This sets the triple channel apart from the others, where the binary shrinks by giving its energy to the reservoir (the cluster, the AGN or the envelope of its companion); in the triple channel, energy is not exchanged with the outer orbit—only angular momentum (in other dynamical channels angular momentum is of course exchanged, too, but energy also is).[2] Once the inner binary becomes eccentric enough, it releases its energy directly into gravitational waves.

The paper is organised as follows: we start by describing an analytical map that models the evolution of the orbital elements of a quasi-hierarchical triple in §2, which we then show leads to a somewhat different maximum secular eccentricity than ZLK oscillations (§3), and we comment on its consequences for gravitational-wave coalescences. Then, we consider the long-term evolution of triples under the map, approximating as a random walk in §4, and describe some of its consequences. We conclude by summarising our findings in §5.

2 EVOLUTION OF QUASI-HIERARCHICAL TRIPLES

As remarked in the introduction (§1), a quasi-hierarchical triple is a triple system where the semi-major axis $a_{\rm in}$ of the inner binary (composed of masses m_1 and m_2) is much smaller than that of the outer binary (comprising the inner binary's centre of mass and the mass m_3), denoted by $a_{\rm out}$; however, the eccentricity of the tertiary's orbit about the inner binary centre-of-mass is so large, that its periapsis, $r_{\rm p} \equiv r_{\rm p,out}$ is not much smaller than $a_{\rm in}$. Thus, we have

$$1 \lesssim \frac{r_{\rm p}}{a_{\rm in}} \ll \frac{a_{\rm out}}{a_{\rm in}}. \tag{1}$$

In this case, the inner binary's evolution is dominated by the 'impulsive kicks' it receives during each pericentre passage of the outer object (Antonini et al. 2010). Each of these close encounters is similar to an interaction of a binary with an unbound perturber on a parabolic orbit, whose distance of closest approach is $r_{\rm p}$; such close encounters have already been studied in the literature by Heggie & Rasio (1996); Hamers & Samsing (2019a,b). Here, the binary evolves under a sequence of such kicks, which are correlated with each other, in the sense that they are all determined by the same outer orbit.

The system is still hierarchical, so one may average the interaction between the binary and the outer body over the period of the inner binary—but not over the period of the outer. This implies that the energy of the inner binary is

[2] Although an energy exchange may occur in gaseous environment (Su et al. 2025).

Main dynamical evolution	range of $e_{\rm out}$	probability for thermal distribution (with $a_{\rm out} = 100a_{\rm in}$)	
Secular	$1 - e_{\rm out} \geq \sqrt{a_{\rm in}/a_{\rm out}}$	$\mathcal{O}(1)$	(81%)
Quasi-hierarchical (this work)	$\sqrt{a_{\rm in}/a_{\rm out}} \geq 1 - e_{\rm out} \geq a_{\rm in}/a_{\rm out}$	$\mathcal{O}(\sqrt{a_{\rm in}/a_{\rm out}})$	(17%)
Unstable (strong triple scattering)	$1 - e_{\rm out} \leq a_{\rm in}/a_{\rm out}$	$\mathcal{O}(a_{\rm in}/a_{\rm out})$	(2%)

Table 1. Three regimes for dynamical triple evolution. The right column displays the relative probability of being in each one, for a thermal distribution of $e_{\rm out}$ ($p(e_{\rm out}) = 2e_{\rm out}$), and $a_{\rm in}/a_{\rm out} = 0.01$.

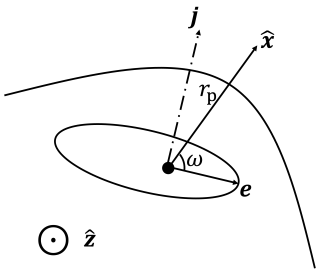

Figure 1. A depiction of the orientations of the three bodies (see text and equations (2)). The $\hat{\mathbf{x}}$-axis points from the binary's centre-of-mass to the outer pericentre, and the $\hat{\mathbf{z}}$-axis points out of the page.

conserved, but its angular momentum is not. The latter is characterised by the Laplace–Runge–Lenz vector

$$\mathbf{e} \equiv e \begin{pmatrix} \cos\Omega\cos\omega - \sin\Omega\sin\omega\cos i \\ \sin\Omega\cos\omega + \cos\Omega\sin\omega\cos i \\ \sin i\sin\omega \end{pmatrix}, \tag{2}$$

and the dimension-less angular momentum

$$\mathbf{j} \equiv \sqrt{1-e^2} \begin{pmatrix} \sin\Omega\sin i \\ -\cos\Omega\sin i \\ \cos i \end{pmatrix}, \tag{3}$$

where $i \equiv \arccos(\mathbf{j}\cdot\hat{\mathbf{z}})$ and have adopted the angle conventions of Hamers & Samsing (2019a), where the outer angular momentum is always $\mathbf{J}_{\rm out} \parallel \hat{\mathbf{z}}$. We fix the outer orbit's orientation as depicted in figure 1. With the semi-major axis $a_{\rm in}$ and the masses being fixed, $\mathbf{e}$ and $\mathbf{j}$ determine the inner binary's orbit completely. After each close pericentre passage of the outer body, $\mathbf{e}$ changes by an amount $\Delta\mathbf{e}$, and $\mathbf{j}$ changes by $\Delta\mathbf{j}$. The magnitude of these changes is determined by the hierarchy parameter (Hamers & Samsing 2019a)

$$\varepsilon \equiv \sqrt{\frac{m_3^2}{m_b M}\left(\frac{a_{\rm in}}{r_{\rm p}}\right)^3}, \tag{4}$$

where $m_{\rm b} \equiv m_1 + m_2$ is the inner binary's mass and $M \equiv m_{\rm b} + m_3$ is the total mass. We denote the inner (outer) reduced mass by $\mu_{\rm in}$ ($\mu_{\rm out}$).

Furthermore, because $r_{\rm p} \ll a_{\rm out}$, we may approximate the outer eccentricity as $e_{\rm out} \approx 1$; that is, we will treat each of the close pericentre passages as a parabolic encounter. Under this assumption,

$$\begin{aligned} \Delta\mathbf{e} &= \frac{3\pi}{2}\varepsilon \begin{pmatrix} -e_z j_y - e_y j_z \\ e_z j_x + e_x j_z \\ 2e_y j_x - 2e_x j_y \end{pmatrix} + \varepsilon^2 \mathbf{g}_e, \\ \Delta\mathbf{j} &= \frac{3\pi}{2}\varepsilon \begin{pmatrix} -j_y j_z - 5e_y e_z \\ 5e_x e_z - j_x j_z \\ 0 \end{pmatrix} + \varepsilon^2 \mathbf{g}_J, \end{aligned} \tag{5}$$

where the second-order corrections $\mathbf{g}_e$ and $\mathbf{g}_J$ are given by equation (27) of Hamers & Samsing (2019a), at quadrupole order. In particular, the change in eccentricity, $\Delta e = (\mathbf{e}\cdot\Delta\mathbf{e})/e$ reads

$$\begin{aligned} \Delta e = {} & \frac{15\pi}{4}\varepsilon e\sqrt{1-e^2}\sin^2 i \sin 2\omega + \frac{9\pi^2}{512}\varepsilon^2 e\left(124 - 299e^2\right) \\ & + \frac{3\pi}{512}\varepsilon^2 e\Big\{100\left(1-e^2\right)\sin 2\omega\big[(5\cos i + 3\cos 3i)\cos 2\Omega \\ & + 6\sin i \sin 2i\big] + 4\cos 2i\left[200\left(1-e^2\right)\cos 2\omega \sin 2\Omega \right. \\ & \left. + 3\pi\left(81e^2 - 56\right)\right] + 3\pi\left[200e^2\sin^4 i\cos 4\omega \right. \\ & \left. + 8\left(16e^2+9\right)\sin^2 2i\cos 2\omega + \left(39e^2+36\right)\cos 4i\right]\Big\}. \end{aligned} \tag{6}$$

The evolution of the system is therefore approximated by a sequence of N parabolic encounters, each of which change the inner binary orbit as

$$\begin{aligned} a_{n+1} &= a_n, \\ \mathbf{e}_{n+1} &= \mathbf{e}_n + \Delta\mathbf{e}(a_n, e_n, i_n, \omega_n, \Omega_n), \\ \mathbf{j}_{n+1} &= \mathbf{j}_n + \Delta\mathbf{j}(a_n, e_n, i_n, \omega_n, \Omega_n). \end{aligned} \tag{7}$$

We account for angular-momentum conservation explicitly, and for the possibility of orbit flips as explained in appendix A. In that appendix, we also describe our implementation of the method of McGuire et al. (2026) to account for the phase-space constraints $\mathbf{e}\cdot\mathbf{j} = 0$ and $e^2 + j^2 = 1$.

This approach is empirically found to be valid for $r_{\rm p} \gtrsim 3a_{\rm in}$ (Samsing et al. 2019) in the case of a single pericentre passage; below this ratio, even the single-averaging over the inner binary is inadequate, so energy exchanges need to be accounted for, and incorporated into the kicks (Mushkin & Katz 2020). We do not consider such cases here, and restrict ourselves to the case where averaging over the inner binary's orbit—and hence $a_{n+1} = a_n$—is still acceptable. Appendix A provides more details of the behaviour of Δe engendered by this map, as a function of the various angles involved.

3 SECULAR OSCILLATIONS

The map (7) leads to secular oscillations of e_n. Figure shows a comparison of the outcome of applying it to a numerical integration of the equations of motion with direct three-body simulations.

We compare the analytical prescription to three-body simulations run with the `rebound` code (Rein & Liu 2012; Rein & Tamayo 2015), using the `ias15` integrator, with the following configuration: $m_1 = m_2 = m_3 = M_\odot$, $a_{\rm in} = 1$AU, $a_{\rm out} = 1000a_{\rm in}$, $e_{\rm out} = 0.99$, $i_0 = \pi/2$, $\omega_0 = \Omega_0 = \pi/4$.

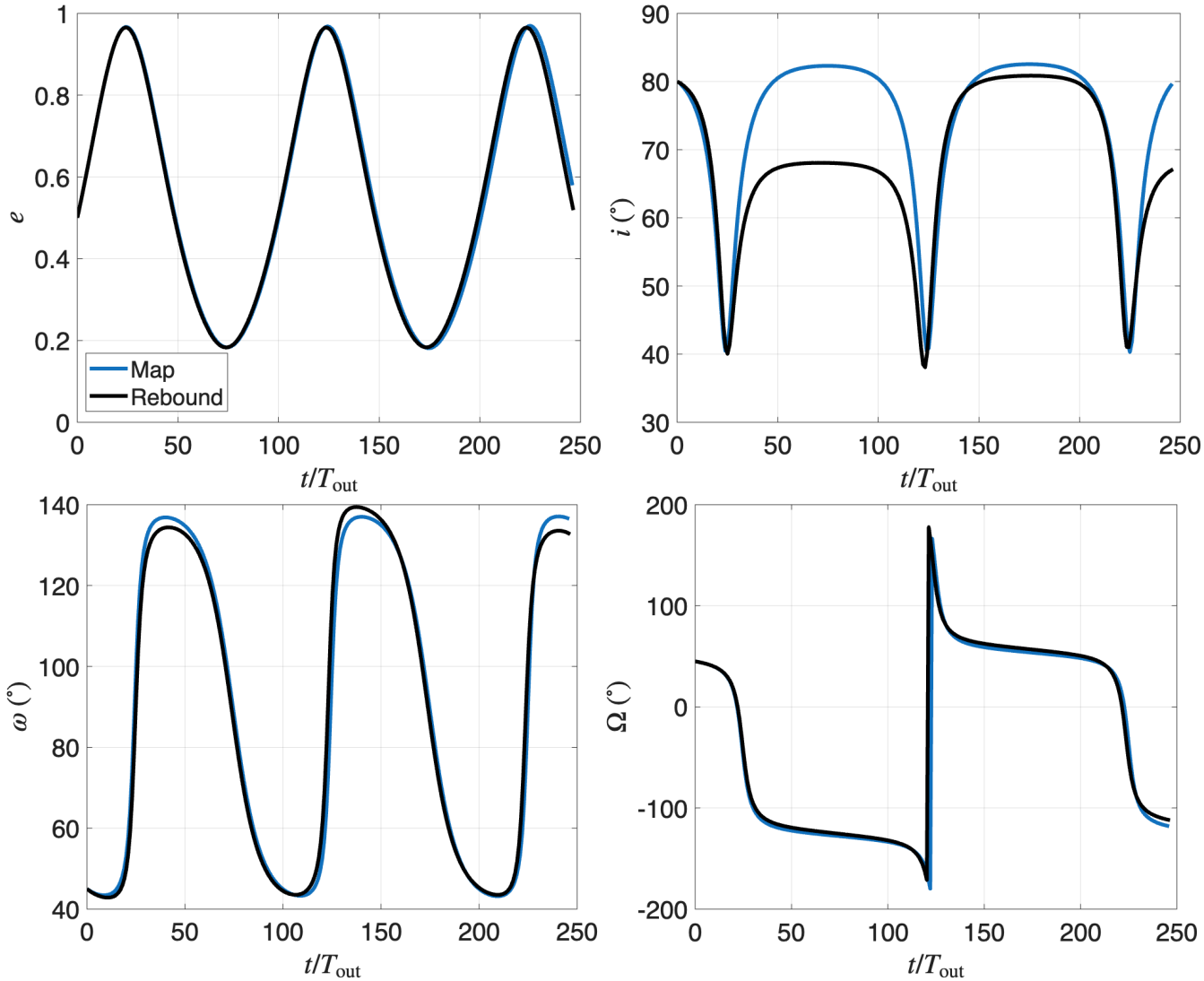

Figure 2. A comparison between the analytical map (blue) $\Delta\mathbf{e}$, $\Delta\mathbf{j}$ given in equations (5–7), and the results of a direct three-body simulation (in black, dash-dotted); see text for details. We see that the simulations matches the analytical formula well. We ascribe the disagreement in inclination to a different way of defining it in `rebound`.

We run the code for 250 outer orbits, and compare the evolution of orbital parameters of the inner orbit with those predicted by equations (7). The comparison, showing good agreement over many outer orbits—for both the magnitude of the changes and the time-scale—is displayed in figure 2.[3] While we do not plot $a_{\rm in}$ over multiple outer-pericentre passages, the `rebound` simulations do conserve it as expected. We see that the map traces the evolution of the system faithfully for hundreds of outer orbits—a few secular cycles. Then, the two descriptions start to deviate. The discrepancy arises from the impact of $\mathcal{O}(\varepsilon^3)$ and $\mathcal{O}(1-e_{\rm out})$ terms that we have neglected, over long times.

The secular time-scale can be immediately gleaned from equation (6):

$$\frac{T_{\rm out}}{\tau_{\rm sec}} \sim \frac{15\pi\varepsilon e\sqrt{1-e^2}\sin^2 i}{4} + \frac{9\pi^2}{512}\varepsilon^2 e \times \left[4(81e^2-56)\cos 2i + (39e^2+36)\cos 4i - 299e^2 + 124\right] , \tag{8}$$

where the second line matters mostly for $i \sim 0°, 180°$, for it is otherwise smaller than the first. To leading order,

$$\tau_{\rm sec} \sim T_{\rm out}\frac{\sqrt{m_b M}}{m_3 e\sqrt{1-e^2}\sin^2 i}\left(\frac{r_{\rm p}}{a_{\rm in}}\right)^{3/2} ; \tag{9}$$

this is the eccentric ZLK time-scale, divided by the denominator $e\sqrt{1-e^2}\sin^2 i$.

We can compute the maximum eccentricity $e_{\rm max}$ that the triple can achieve over a secular cycle, by a repeated iteration of equation (7). This can be compared with predictions

[3] We believe the discrepancy in the inclination to arise from an inconsistency between our definition for it, and the one used in `rebound`. We did attempt to understand if this is indeed a geometric problem, but were unable to find a corrected definition that resolved it. We still suspect it to be the case, though, because all other angles agree very well, and because the inclination does return to agreement with the map after about $120T_{\rm out}$.

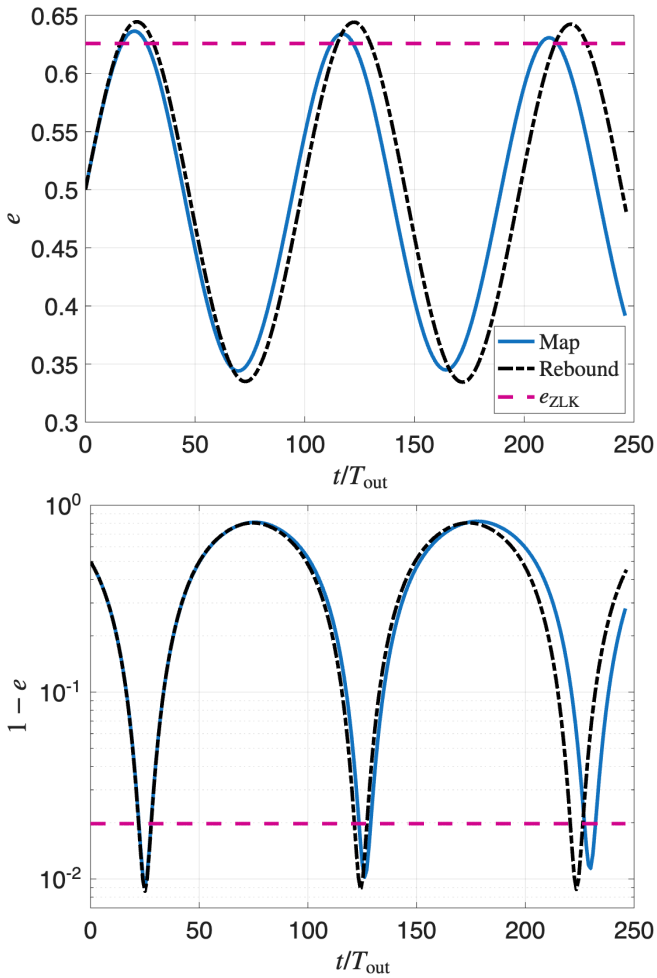

Figure 3. The evolution of a quasi-hierarchical orbit over a few secular times, from the map (7) (blue) and `rebound` (black), for $m_1 = m_2 = m_3 = M_\odot$, $\omega_0 = \Omega_0 = \pi/4$, $r = 10a_{\rm in}$, $a_{\rm out} = 1000a_{\rm in}$; *top*: $i_0 = 7\pi/9$, *bottom*: $i_0 = 5\pi/9$. The purple curve shows is the maximum eccentricity according to pure quadrupole ZLK evolution.

from the quadrupole ZLK mechanism (e.g. Naoz 2016; Hamilton & Rafikov 2019). As seen from an example in figure 3, quasi-hierarchical triples sometimes exceed the ZLK maximum eccentricity.

In figure 4 we explore how the value of $e_{\rm max}$ depends on the initial eccentricity and inclination. As can be seen from the right panel, the deviation is sometimes significant. The difference in maximum eccentricity leads to a difference in the time to coalescence due to gravitational-wave emission. For an orbit with eccentricity e, it is given by

$$\tau_{\rm gw} = \tau_{\rm c}\left(1-e^2\right)^{7/2}\,, \tag{10}$$

where $\tau_{\rm c}$ is the time-to-coalescence of a circular binary, given by (Maggiore 2008)

$$\tau_{\rm c} = \frac{5}{256}\frac{c^5 a_{\rm in}^4}{G m_{\rm c}^{5/3} m_{\rm b}^{4/3}}\,. \tag{11}$$

Liu & Lai (2017, 2018) argued that given the strong dependence of $\tau_{\rm gw}$ on the eccentricity, one could approximate the entire energy loss as occurring near pericentre. As e fluctuates, the only time any significant GW emission occurs, is when $e \sim e_{\rm max}$. Thus, according to Liu & Lai (2017, 2018), the time a binary, undergoing secular oscillations, takes to coalesce is well approximated by

$$t_{\rm coal} \approx \tau_{\rm c}\left(1-e_{\rm max}^2\right)^{7/2}\frac{T(e\sim e_{\rm max})}{\tau_{\rm sec}(\text{low } e)}\,, \tag{12}$$

where $T(e \sim e_{\rm max})$ is the time the secular oscillations spend with e near $e_{\rm max}$. For ZLK evolution this is $\tau_{\rm sec}(\text{low } e)\sqrt{1-e_{\rm max}^2}$, and here, we estimate it as follows: for strong GW emission we need $e_{\rm max} - e \ll 1 - e_{\rm max}$, whence equation (6) implies that here

$$T(e\sim e_{\rm max}) \sim \tau_{\rm sec}(\text{low } e)\frac{\sqrt{1-e_{\rm max}^2}}{e_{\rm max}}\sin^2 i(e_{\rm max})\,, \tag{13}$$

retaining the same $\sqrt{1-e_{\rm max}^2}$ dependence as the ZLK case. Therefore, neglecting the inclination dependence, the Liu & Lai (2017, 2018) relation $t_{\rm coal} = \tau_{\rm c}\left(1-e_{\rm max}^2\right)^3$ obtains here, too; quantitatively, it is modified by

$$\frac{t_{\rm coal,ZLK}}{t_{\rm coal}} \approx 1+\delta_{\rm max} \equiv \left(\frac{1-e_{\rm ZLK}^2}{1-e_{\rm max}^2}\right)^3\,. \tag{14}$$

This is plotted in figure 5. The deviation is largest around $i_0 \sim 90^\circ$, because that's where $t_{\rm coal}$ is shortest, and can be significant.

4 EXTERNAL EFFECTS AND POSSIBLE ECCENTRICITY DRIFT

The angular-momentum changes accumulate over long times, leading to a quasi-random behaviour of the map (7), as can be shown in figure 6. This figure was created using random initial conditions, with $r_{\rm p} = 10a_{\rm in}$, and equal binary masses. We terminate the evolution once e_n reaches 1. We display five example trajectories.

4.1 Pure evolution under the map

Let us construct a useful model for understanding the evolution of the system, under equations (7). We see from figure 6 that **e** and **j** explore their available phase-space, with ω and Ω varying wildly from one encounter to the next. Indeed, if the angles ω and Ω change sufficiently fast, then these rapid (in comparison with the changes in e and i) fluctuations may be approximated as random. This is of course only true on long time-scales, of the order $\tau_{\rm sec}$. Equations (7) then imply that the motion of e and i can be approximated as a partially-random walk, where, in each step, ω_n and Ω_n are essentially random, and the jumps are given by equations (5). This walk is correlated in the sense that on short time-scales (the time it takes ω or Ω to scramble), e and i retain memory of their previous states.

4.2 External perturbations

The true evolution of the triple does not display such an eccentricity drift. This is because the triple does not evolve with a random Ω and ω at every time-step. For example, at $\mathcal{O}(\varepsilon)$, j_z and the single-averaged Hamiltonian are conserved, meaning that the triple's evolution is integrable, leading to periodic motion. The `rebound` simulation is also periodic, as

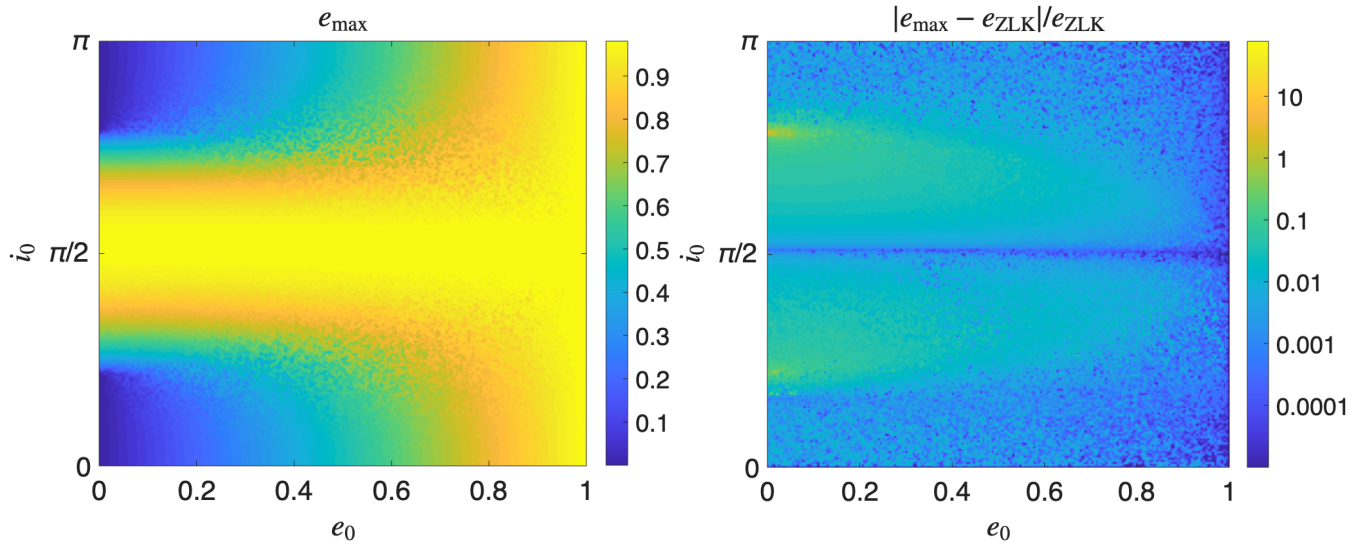

Figure 4. *Left*: a diagram of the maximum eccentricity achieved by a quasi-hierarchical triple over an $\mathcal{O}(\tau_{\rm sec})$ time-scale, found as the first local eccentricity maximum, for equal masses. *Right*: a comparison with the maximum eccentricity according to pure (quadrupole) ZLK evolution; the colour-scheme is logarithmic. See text for details.

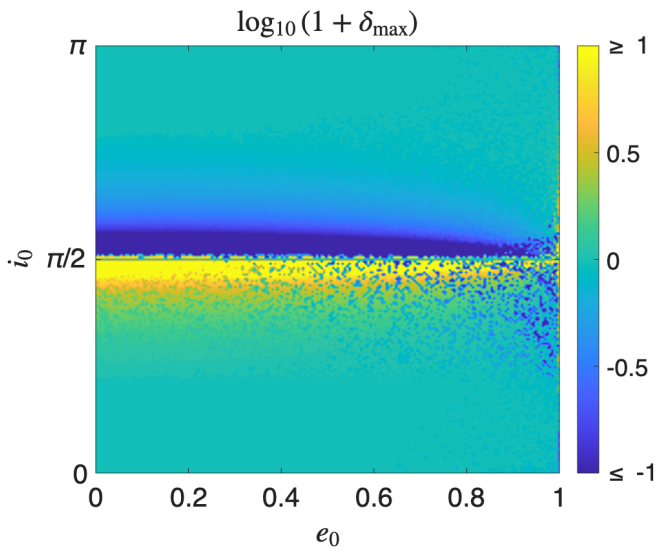

Figure 5. The change in the time to coalescence from standard ZLK evolution, from equation (14). The change is stronger around $i_0 = \pi/2$, where both $e_{\max}$ and $e_{\rm ZLK}$ are very high.

can be seen in figure 7, which indeed does not display an eccentricity drift. We thus conclude that quasi-hierarchical triples of point particles, without general relativity, which are in isolation, exhibit periodic behaviour.

However, it is interesting to ask if there are astrophysical systems where the triple's evolution does display a quasi-random eccentricity drift, e.g. if there is an extra randomness on a time-scale $\tau_{\rm sec}$. This can occur, for example, in the context of relativistic phase-space diffusion (Kuntz 2022; Hamilton & Rafikov 2024), or if the outer orbit is itself subject to perturbations, which can change i and Ω, e.g. from by-passing stars (Hamers et al. 2018), a fourth object (e.g., Yang et al. 2025, figure 6) or tri-axiality of the external potential (Petrovich & Antonini 2017), where it is known that the inner eccentricity can experience a drift to ever higher values and that eccentricities experience a diffusion. A related study by Winter-Granic et al. (2024), saw an enhancement of the probability of reaching very high eccentricities if both galactic tides and fly-bys perturb a binary, rather than just one of these processes.

There is a possibility that the outer angular momentum would shrink to such a value that $r_{\rm p,out}$ would cease to be larger than $\sim a_{\rm in}$, thereby violating the quasi-hierarchical assumption made in this paper. Indeed, if that occurs, the conclusions of this section would not apply. However, generically, the time-scale for the *direction* of the outer orbit to diffuse is shorter than the time-scale for it to change its magnitude (e.g. in the case of by-passing stars, leading to vector resonant relaxation being more rapid than its scalar counterpart; Kocsis & Tremaine 2011; Hamers et al. 2018); in that case, the outer angular momentum can change without violating this assumption. For example, if Ω is subject to a random change in each outer orbit, then the map (7) will lead to a random walk of $\mathbf{e}$ and i. The bottom right panel of figure 6 shows why that is: Ω essentially changes by an $\mathcal{O}(\pi)$ amount over one secular time, so over many secular times, its value (modulo 2π) is essentially random; hence, if the true evolution randomises Ω over a secular time, the effect on the inner binary will be qualitatively the same as if Ω were randomised by the map (with its $\mathcal{O}(\varepsilon^3)$ errors leading to non-periodic evolution).

Let us now postulate that such a triple exists, where Ω experiences random perturbations on a $\tau_{\rm sec}$ time-scale. These can be more or less arbitrary, in-so-far as they remove any additional constraints that equations (7) do not satisfy, that the exact, isolated triple does. We therefore assume here, that if constraints on the angular-momentum direction of the outer orbit are removed—manifesting in, e.g., a random changes in Ω, thought of as coupling the outer orbit to a bath with which it can exchange angular momentum—the triple evolves qualitatively as in equations (7). Essentially, we take the outer orbit to be a different one each time-step, but with the same

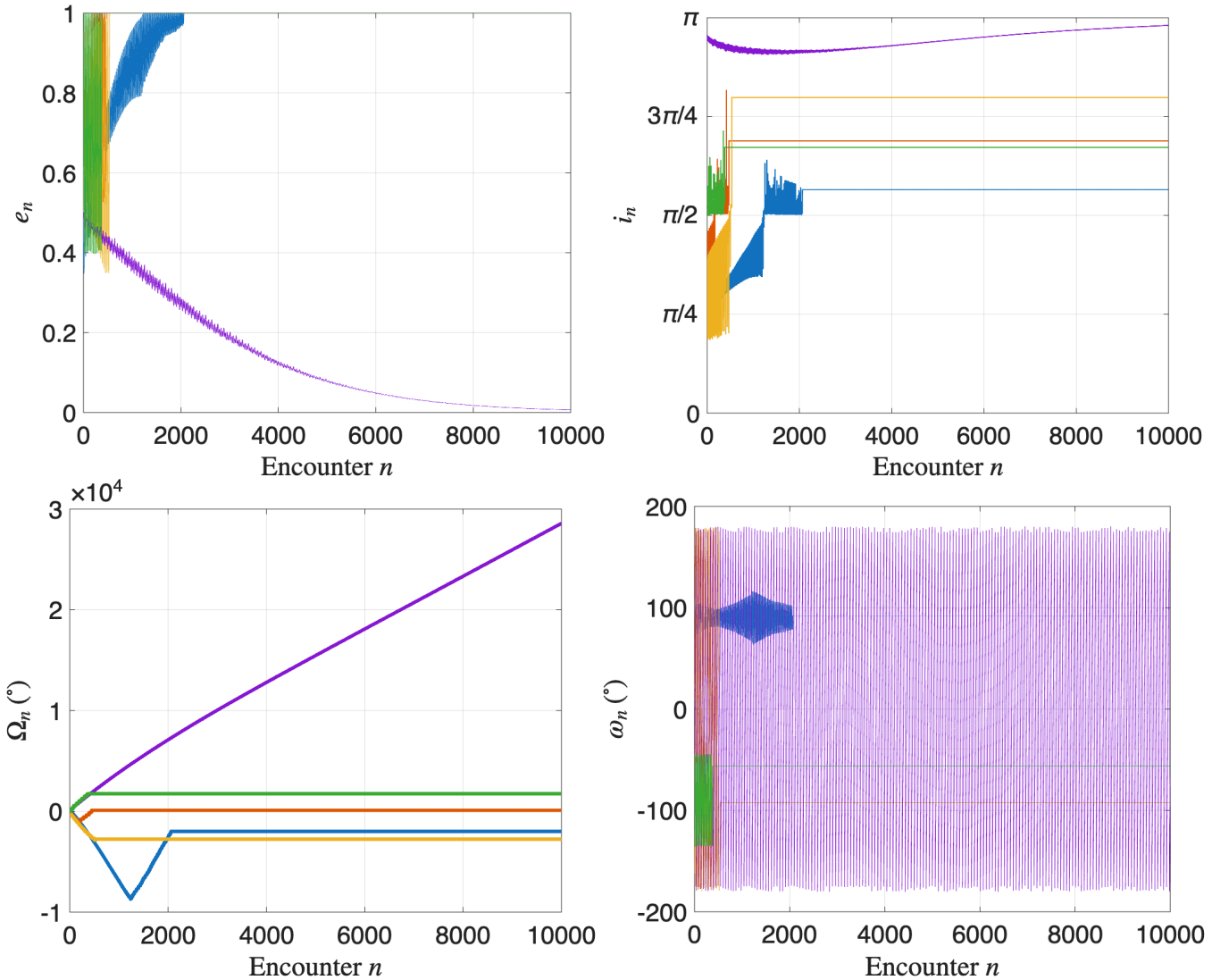

Figure 6. The evolution of randomly chosen initial conditions, for an equal-mass triple, for 10000 outer orbits, and $r_{\rm p} = 10a_{\rm in}$, as determined by equations (5). The system is frozen when e_n reaches 0.9999. See text and appendix A for details. The colours correspond to five random realisations of the initial conditions, and are consistent across the four panels.

values of $r_{\rm p,out}$ and i. Thus, each time-step is essentially a new parabolic encounter.

Let us focus on e for such a hypothetical triple: its random walk has two boundaries $e_{\rm l} = 0$ and $e_{\rm u} = 1$ (this can be replaced by any value $e_{\rm u} = e_{\rm coll}$ above which a collision occurs, or the inner binary coalesces much more quickly than an outer orbital period). The first-order part of Δe has zero average (over ω and Ω), and its second moment is

$$\sqrt{\langle \Delta e^2 \rangle} = \frac{15\pi}{4\sqrt{2}} \varepsilon e \sqrt{1-e^2} \sin^2 i + \mathcal{O}(\varepsilon^2). \tag{15}$$

Thus, it appears that the walk would inevitably reach the boundary—either $e = e_{\rm u}$ (where it would terminate) or at $e = 0$ (where it stalls).

There is another drift term, which can overcome the diffusion: consider equation (6), when averaged over ω and Ω, *viz.*

$$\langle \Delta e \rangle = \frac{9\pi^2}{512} \varepsilon^2 e \Big[4(81e^2 - 56)\cos 2i + (39e^2 + 36)\cos 4i - 299e^2 + 124 \Big]. \tag{16}$$

At i close to 0 and π, the first-order diffusion (15) is negligible, and hence the eccentricity changes are dominated by this $\langle \Delta e \rangle$. For $i > \pi - \arctan\left(\frac{\sqrt{\sqrt{97}-1}}{2\sqrt{6}}\right)$, this drift is negative for all e, whence it seems that sufficiently retrograde orbits would consistently lose eccentricity under such an evolution. We show in appendix B that this is indeed the case. The boundary between the region where e can walk randomly to high eccentricities is given by requiring that i_0 be sufficiently close to $\pi/2$, for an orbital flip to be possible within one secular period, i.e.,

$$\frac{1}{\varepsilon} \Delta j_z \sim j_z \,, \tag{17}$$

where Δj_z is maximised over all values of ω and Ω. If $i_0 -$

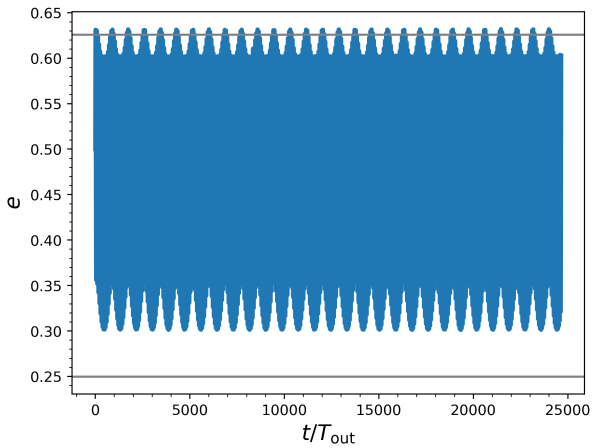

Figure 7. The eccentricity evolution for the example parameters: $m_1 = 1.9\,M_\odot$, $m_2 = 0.1\,M_\odot$, $m_3 = M_\odot$, $r_\mathrm{p} = 7a_\mathrm{in}$, $i_0 = 7\pi/9$, from `rebound`.

$\pi/2 \ll 1$, this simplifies to

$$i_0 \leq i_\mathrm{crit} \equiv \pi - \arccos\left(\min\left\{1, \frac{300\pi\sqrt{1-e^2}\varepsilon}{64(1-e^2)}\right\}\right) . \tag{18}$$

We verify this in appendix B.

Near the boundary $e = 0$, we have $\Delta e \sim e$. This means that even if all changes Δe_n are negative (an event with an exponentially small probability), e cannot decrease faster than as a geometric sequence—it does not reach $e = 0$ at a finite time. Hence, for $i_0 \leq i_\mathrm{crit}$ the walker, if starting at $e_0 > 0$, never reaches $e = 0$ exactly. For $i_0 \geq i_\mathrm{crit}$, the negative drift eventually wins, causing i to approach π and e to tend asymptotically to 0.

This behaviour is in contrast with the boundary e_u, where equation (6) yields $\Delta[1-e] \sim \sqrt{1-e}$, whence here, if steps do add up coherently, e can reach $e = e_\mathrm{u}$ in a finite time.[4] In conclusion, the boundary at $e = 0$ is benign, and can never be reached at a finite time, while the boundary $e = e_\mathrm{u}$ can be. Therefore, the upper boundary, at $e = e_\mathrm{u}$, will inevitably be reached for $i_0 \leq i_\mathrm{crit}$, for every initial non-zero eccentricity. Observe that it is impossible for Δe to be larger than $1-e$; this is both a property of equation (6), and an immediate consequence of orbit-averaging over the inner orbit. Such orbit-averaging was shown to be an excellent approximation as long as $r_\mathrm{p} \geq 3a_\mathrm{in}$ (Hamers & Samsing 2019a; Samsing et al. 2019) for individual parabolic encounters.

As we are agnostic here about the astrophysical environment that leads, in reality, to a randomisation of Ω or ω, we leave a more detailed study of the long-term evolution under the map (7), and its consequences, to appendix B.

5 DISCUSSION AND SUMMARY

In this paper, we analysed the dynamical evolution of quasi-hierarchical triples, where there is a clear hierarchy between the orbital times of the outer and the inner orbits, but the outer eccentricity is so high, that the outer orbit's time at pericentre is not as significantly larger than the inner orbital period. We modelled these systems using a map—from one outer pericentre to the next—where each step was approximated as a parabolic encounter between the inner binary and the tertiary companion. These steps were of course correlated, because it is the same tertiary that encounters the same binary. The orbital evolution displays secular oscillations of $\mathbf{e}$ and $\mathbf{j}$, qualitatively similar to ZLK oscillations. However, the orbit is sometimes capable of reaching an even larger maximum eccentricity, or a lower one, than what is predicted by pure ZLK evolution. These deviations are present at second-order quadrupole order, occurring on a quadrupole time-scale, even for equal masses, where the octupole vanishes. We showed that such a modelling agrees with direct three-body integration over secular times.

Over many secular times, the map (7) accrues $\mathcal{O}(\varepsilon^3)$ errors, which cause it to deviate from numerical integration. Instead, that map causes the angles ω and Ω to fluctuate significantly during these kicks, so the evolution of e and i can be approximated as a random walk. This behaviour is not present in isolated quasi-hierarchical triples, but we hypothesise that it can arise if the outer orbit is not forced to conserve its angular momentum—if the outer orbit is weakly coupled to a system with which is can exchange angular momentum. This implies that, e.g., Ω is randomised between kicks, so the inner orbit's evolution is that same as what would happen under consecutive interactions with *different* outer, parabolic orbits.

If indeed the map (7) is a reasonable approximation in that case, we showed that this walk inevitably leads to e reaching arbitrarily large values, and that it necessarily eventually reaches the boundary $e = 1$. The time to do so was found in appendix B to be the diffusion time-scale $t_\mathrm{max} = \tau f(e_0, i_0|e_\mathrm{u})$, which we showed scaled like ε^{-2}. We leave a quantitative study of the applicability of the random-walk model to non-isolated triples for future work.

Applications for this theory include—but are not limited to—an enhancement of the triple channel from gravitational-wave source formation. For isolated triples, the time it takes the inner binary to coalesce is modified by an additive factor δ_max, plotted in figure 5. For triples where the map (7) is a faithful qualitative description of their long-term evolution, the diffusion process speeds up the time to reach high eccentricities significantly, driving the inner binary all the way to small pericentres, where relativistic precession and/or emission become stronger than quasi-hierarchical evolution. In systems which obey the hierarchy (1) but not the stronger condition (B3), one must account both for the quasi-hierarchical 'jumps' due to outer-pericentre passages, and for the deterministic secular contribution of the rest of the outer orbit, on $\mathcal{O}(T_\mathrm{out}/\varepsilon^2)$ times. That is, the map (7) must be modified to include, e.g. the changes in $\mathbf{e}$ and $\mathbf{j}$ induced by the ZLK effect, in addition to those in (5). This combined treatment is left for future work.

ACKNOWLEDGEMENTS

We are grateful to Francesco Mori for helpful discussions on random walks, to Evgeni Grishin and Mor Rozner for very helpful comments on the manuscript, and to Samuel Macguire and Evgeni Grishin for sharing their implementation of the Hamers & Samsing (2019a) equations in McGuire et al. (2026). We thank Mor Rozner for her encourage-

[4] This may be formalised using a Grönwall (1919)-like estimate.

ment to finish the paper. We thank the anonymous referee for their helpful comments, which improved the manuscript. This work was supported by a Leverhulme Trust International Professorship Grant (No. LIP-2020-014). The work of Y.B.G. was partly supported by a Simons Investigator Award to A.A. Schekochihin (No. 930121). J. Samsing's work was partly supported by the ERC Starting Grant No. 121817-BlackHoleMergs (PI: Samsing) and by the Villum Foundation (Villum Fonden; grant No. 29466). The Centre of Gravity at the Niels Bohr Institute is a Centre of Excellence funded by the Danish National Research Foundation under grant No. 184.

DATA AVAILABILITY

Simulations conducted for this article utilised the publicly available code `rebound` (Rein & Liu 2012; Rein & Tamayo 2015).[5] Scripts and input files used to make the figures in this article will be shared upon reasonable request to the corresponding author.

REFERENCES

Antognini J. M., Shappee B. J., Thompson T. A., Amaro-Seoane P., 2014, MNRAS, 439, 1079
Antonini F., Rasio F. A., 2016, ApJ, 831, 187
Antonini F., Faber J., Gualandris A., Merritt D., 2010, ApJ, 713, 90
Antonini F., Murray N., Mikkola S., 2014, ApJ, 781, 45
Antonini F., Chatterjee S., Rodriguez C. L., Morscher M., Pattabiraman B., Kalogera V., Rasio F. A., 2016, ApJ, 816, 65
Antonini F., Toonen S., Hamers A. S., 2017, ApJ, 841, 77
Antonini F., Romero-Shaw I. M., Callister T., 2025, Phys. Rev. Lett., 134, 011401
Arnold V. I., Kozlov V. V., Neishtadt A. I., 2006, Mathematical aspects of classical and celestial mechanics, third edn. Encyclopaedia of Mathematical Sciences Vol. 3, Springer-Verlag, Berlin
Bartos I., Kocsis B., Haiman Z., Márka S., 2017, ApJ, 835, 165
Bartos I., Rosswog S., Gayathri V., Miller M. C., Veske D., Marka S., 2023, arXiv e-prints, p. arXiv:2302.10350
Belczynski K., Kalogera V., Bulik T., 2002, ApJ, 572, 407
Belczynski K., Holz D. E., Bulik T., O'Shaughnessy R., 2016, Nature, 534, 512
Binney J., Tremaine S., 2008, Galactic Dynamics: Second Edition. Princeton University Press
Dominik M., Belczynski K., Fryer C., Holz D. E., Berti E., Bulik T., Mandel I., O'Shaughnessy R., 2012, ApJ, 759, 52
El-Badry K., Rix H.-W., 2018, MNRAS, 480, 4884
Fabj G., Samsing J., 2024, arXiv e-prints, p. arXiv:2402.16948
Ford E. B., Kozinsky B., Rasio F. A., 2000, ApJ, 535, 385
Fragione G., Loeb A., 2019, MNRAS, 486, 4443
Fragione G., Grishin E., Leigh N. W. C., Perets H. B., Perna R., 2019, MNRAS, 488, 47
Gilbaum S., Grishin E., Stone N. C., Mandel I., 2025, ApJ, 982, L13
Ginat Y. B., Perets H. B., 2021, Physical Review X, 11, 031020
Ginat Y. B., Perets H. B., 2023, MNRAS, 519, L15
Grishin E., 2024, MNRAS, 533, 486
Grishin E., Perets H. B., 2022, MNRAS, 512, 4993
Grishin E., Perets H. B., Fragione G., 2018, MNRAS, 481, 4907
Grishin E., Gilbaum S., Stone N. C., 2024, MNRAS, 530, 2114
Grönwall T. H., 1919, Annals of Mathematics, 20, 292
Hamers A. S., Samsing J., 2019a, MNRAS, 487, 5630
Hamers A. S., Samsing J., 2019b, MNRAS, 488, 5192
Hamers A. S., Bar-Or B., Petrovich C., Antonini F., 2018, ApJ, 865, 2
Hamilton C., 2022, ApJ, 929, L29
Hamilton C., Modak S., 2024, MNRAS, 532, 2425
Hamilton C., Rafikov R. R., 2019, MNRAS, 488, 5512
Hamilton C., Rafikov R. R., 2024, ApJ, 961, 237
Harrington R. S., 1968, AJ, 73, 190
Heggie D. C., 1975, MNRAS, 173, 729
Heggie D. C., Rasio F. A., 1996, MNRAS, 282, 1064
Heinämäki P., Lehto H. J., Valtonen M. J., Chernin A. D., 1999, MNRAS, 310, 811
Heisler J., Tremaine S., 1986, Icarus, 65, 13
Hills J. G., 1980, ApJ, 235, 986
Hut P., 1993, ApJ, 403, 256
Iorio G., et al., 2023, MNRAS, 524, 426
Jiang Y.-F., Tremaine S., 2010, MNRAS, 401, 977
Katz B., Dong S., Malhotra R., 2011, Phys. Rev. Lett., 107, 181101
Klein Y. Y., Katz B., 2024, MNRAS, 535, L31
Kocsis B., Tremaine S., 2011, MNRAS, 412, 187
Kol B., 2021, Celestial Mechanics and Dynamical Astronomy, 133, 17
Kozai Y., 1962, AJ, 67, 591
Kuntz A., 2022, Phys. Rev. D, 105, 024017
Lei H., Grishin E., 2025a, MNRAS, 540, 2422
Lei H., Grishin E., 2025b, MNRAS, 541, 3198
Lidov M. L., 1962, Planetary and Space Science, 9, 719
Liu B., Lai D., 2017, ApJ, 846, L11
Liu B., Lai D., 2018, ApJ, 863, 68
Luo L., Katz B., Dong S., 2016, MNRAS, 458, 3060
Maggiore M., 2008, Gravitational Waves. Vol. 1: Theory and Experiments. Oxford Master Series in Physics, Oxford University Press
Mangipudi A., Grishin E., Trani A. A., Mandel I., 2022, ApJ, 934, 44
Manwadkar V., Trani A. A., Leigh N. W. C., 2020, MNRAS, 497, 3694
Mardling R. A., Aarseth S. J., 2001, MNRAS, 321, 398
Martinez M. A. S., et al., 2020, ApJ, 903, 67
McGuire S., Grishin E., Mandel I., Levin Y., 2026, arXiv e-prints, p. arXiv:2607.18761
McKernan B., Ford K. E. S., O'Shaughnessy R., 2020, MNRAS, 498, 4088
Michaely E., Perets H. B., 2019, ApJ, 887, L36
Michaely E., Perets H. B., 2020, MNRAS,
Monaghan J. J., 1976a, MNRAS, 176, 63
Monaghan J. J., 1976b, MNRAS, 177, 583
Mushkin J., Katz B., 2020, MNRAS, 498, 665
Naoz S., 2016, ARA&A, 54, 441
Naoz S., Farr W. M., Lithwick Y., Rasio F. A., Teyssandier J., 2013, MNRAS, 431, 2155
O'Leary R. M., Kocsis B., Loeb A., 2009, MNRAS, 395, 2127
Offner S. S. R., Moe M., Kratter K. M., Sadavoy S. I., Jensen E. L. N., Tobin J. J., 2023, in Inutsuka S., Aikawa Y., Muto T., Tomida K., Tamura M., eds, Astronomical Society of the Pacific Conference Series Vol. 534, Protostars and Planets VII. p. 275 (`arXiv:2203.10066`), doi:10.48550/arXiv.2203.10066
Perets H. B., 2025, arXiv e-prints, p. 2504.02939
Petrovich C., Antonini F., 2017, ApJ, 846, 146
Portegies Zwart S. F., McMillan S. L. W., 2000, ApJ, 528, L17
Rando Forastier B., Marín Pina D., Gieles M., Portegies Zwart S., Antonini F., 2025, A&A, 697, A118
Raveh Y., Michaely E., Perets H. B., 2022, MNRAS, 514, 4246
Redner S., 2001, A guide to first-passage processes. Cambridge University Press, Cambridge

[5] `https://rebound.readthedocs.io/`

Rein H., Liu S. F., 2012, A&A, 537, A128
Rein H., Tamayo D., 2015, MNRAS, 452, 376
Rodriguez C. L., Antonini F., 2018, ApJ, 863, 7
Rodriguez C. L., Morscher M., Pattabiraman B., Chatterjee S., Haster C.-J., Rasio F. A., 2015, Phys. Rev. Lett., 115, 051101
Rodriguez C. L., Haster C.-J., Chatterjee S., Kalogera V., Rasio F. A., 2016, ApJ, 824, L8
Rowan C., Whitehead H., Fabj G., Saini P., Kocsis B., Pessah M., Samsing J., 2025, MNRAS, 539, 1501
Rozner M., Perets H. B., 2022, ApJ, 931, 149
Samsing J., 2018, Phys. Rev. D, 97, 103014
Samsing J., D'Orazio D. J., 2018, MNRAS, 481, 5445
Samsing J., Hamers A. S., Tyles J. G., 2019, Phys. Rev. D, 100, 043010
Samsing J., et al., 2022, Nature, 603, 237
Samsing J., Hendriks K., Zwick L., D'Orazio D. J., Liu B., 2024, arXiv e-prints, p. arXiv:2403.05625
Saslaw W. C., Valtonen M. J., Aarseth S. J., 1974, ApJ, 190, 253
Shariat C., El-Badry K., Naoz S., 2025, PASP, 137, 094201
Shevchenko I. I., 2017, The Lidov-Kozai Effect - Applications in Exoplanet Research and Dynamical Astronomy. Astrophysics and Space Science Library Vol. 441, Springer, doi:10.1007/978-3-319-43522-0
Stegmann J., Klencki J., 2025, ApJ, 991, L54
Stegmann J., et al., 2024, ApJ, 972, L19
Stone N. C., Leigh N. W. C., 2019, Nature, 576, 406
Stone N. C., Metzger B. D., Haiman Z., 2017, MNRAS, 464, 946
Su Y., Rowan C., Rozner M., 2025, MNRAS, 543, 1864
Tagawa H., Haiman Z., Kocsis B., 2020, ApJ, 898, 25
Tanikawa A., 2013, MNRAS, 435, 1358
The LIGO Scientific Collaboration et al., 2016, Phys. Rev. Lett., 116, 061102
Trani A. A., Spera M., Leigh N. W. C., Fujii M. S., 2019, ApJ, 885, 135
Trani A. A., Tanikawa A., Fujii M. S., Leigh N. W. C., Kumamoto J., 2021, MNRAS, 504, 910
Trani A. A., Rastello S., Di Carlo U. N., Santoliquido F., Tanikawa A., Mapelli M., 2022, MNRAS, 511, 1362
Trani A. A., Quaini S., Colpi M., 2024a, A&A, 683, A135
Trani A. A., Leigh N. W. C., Boekholt T. C. N., Portegies Zwart S., 2024b, A&A, 689, A24
Tremaine S., 2023, MNRAS, 522, 937
Valtonen M., Karttunen H., 2006, The Three-Body Problem. Cambridge University Press, Cambridge
Vigna-Gómez A., et al., 2025, arXiv e-prints, p. 2503.17006
Wen L., 2003, ApJ, 598, 419
Whitehead H., Rowan C., Boekholt T., Kocsis B., 2024, MNRAS, 531, 4656
Will C. M., 2021, Phys. Rev. D, 103, 063003
Winn J. N., Fabrycky D. C., 2015, ARA&A, 53, 409
Winter-Granic M., Petrovich C., Peña-Donaire V., Hamilton C., 2024, ApJ, 973, 53
Yang E., Su Y., Winn J. N., 2025, ApJ, 986, 117
Zhang E., Naoz S., Will C. M., 2023, ApJ, 952, 103
van der Marel R. P., Besla G., Cox T. J., Sohn S. T., Anderson J., 2012, ApJ, 753, 9
von Zeipel E. H., 1910, Astronomische Nachrichten, 183, 345

APPENDIX A: SOME DETAILS ON QUASI-HIERARCHICAL SCATTERING

In this appendix we discuss some features of the quasi-hierarchical interaction between the inner binary and the third star. We also test the approximation by comparing it with the results of a simple three-body simulation.

A1 Magnitude of eccentricity change and angular-momentum flipping

The map (5), applied once, yields a positive or negative eccentricity change, depending on the angles i, ω, Ω and on $r_{\rm p}/a_{\rm in}$. In figure A1 we plot Δe as a function of $1-e_0$, after one outer pericentre, for various values of these parameters. Observe, that $\Delta e \leq 1 - e_0$.

A2 Orbit flipping

A single encounter with the tertiary can also result in i crossing $\pi/2$. However, this occurs when $\Delta\mathbf{j}$ is as large as $\mathbf{j}$, and therefore is not immediately captured by equations (5). To account for it, we first check whether

$$\sqrt{1-e^2} < \frac{15\varepsilon\pi e^2}{4}\,; \tag{A1}$$

if so, then we evolve e via equation (6) as usual; but for the angles, we first evolve i, Ω and ω according to the first-order part of equation (5) (truncated at first order), and then insert those new values into the second-order expressions (5), to obtain i, Ω and ω for the next round. If inequality (A1) is not satisfied, we evolve the orbital parameters as stated in the main text.

This procedure ensures that orbital flipping is correctly accounted for; that this is the appropriate is evident from figure A2, which reproduces the correct flipping results from the three-body simulations of Samsing et al. (2019): this figure should be compared with the top panel of figure 4 of that work, where the orbit flipping was marked based on three-body simulations; the prescription described above reproduces that.

A3 Phase-space constraints

The vectors $\mathbf{e}$ and $\mathbf{j}$ only parameterise a 4D phase-space, spanned by e and the three angles i, ω and Ω, so they satisfy two scalar constraints:

$$e^2 + j^2 = 1\,, \tag{A2}$$

$$\mathbf{e}\cdot\mathbf{j} = 0\,. \tag{A3}$$

The implementation (5) does not necessarily preserve them, exactly. We follow the method proposed by McGuire et al. (2026) in ensuring that they are preserved exactly. In each step, we used equations (5) to advance $\mathbf{e}$ and $\mathbf{j}$. If the new $e^2+j^2 \neq 1$ or $\mathbf{e}\cdot\mathbf{j} \neq 0$, we keep the new value of $\mathbf{e}$ and one component of $\mathbf{j}$, but we solve the two constraint equations for the two other components of $\mathbf{j}$. This introduces $\mathcal{O}(\varepsilon^3)$ changes in just the right way to preserve the constraints. In all cases but $1-e \sim \mathcal{O}(\varepsilon^3)$, there exists a component $j_i \in \{j_x, j_y, j_z\}$ such that the two constraint equations have a real solution for the two other components. We remark that while the improvement of McGuire et al. (2026) is equivalent to the Hamers & Samsing (2019a) map over a single iteration, it yields a dramatic improvement of the agreement with `rebound` over many time-steps.

A4 Angular-momentum conservation

The random walk described in this paper implies that the map (7) tends to bring the inner eccentricity e to higher val-

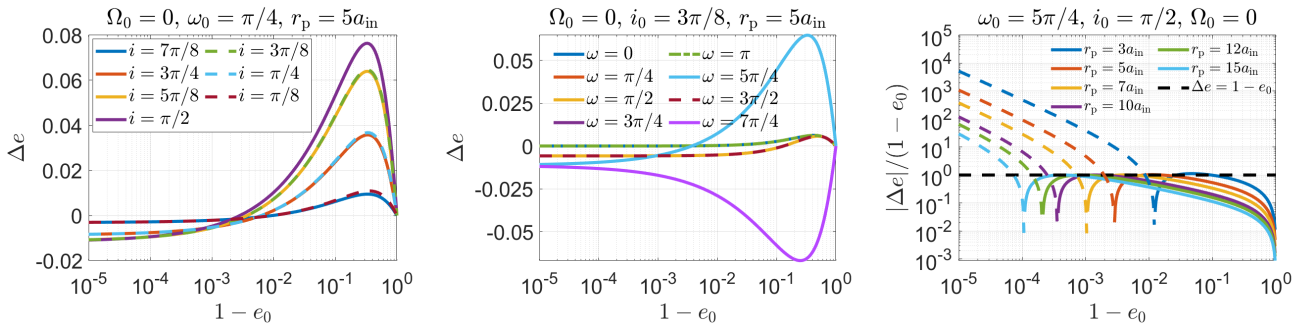

Figure A1. The change Δe in eccentricity, given by equation (6), as a function of the initial eccentricity e_0, for various values of some of the parameters of the problem. *Left*: varying the inclination between the inner and outer orbits; *middle*: varying the inner orbit's argument of pericentre; *right*: varying ε. The dashed lines on the *right* panel correspond to $\Delta e < 0$, while the full lines are $\Delta e \geq 0$.

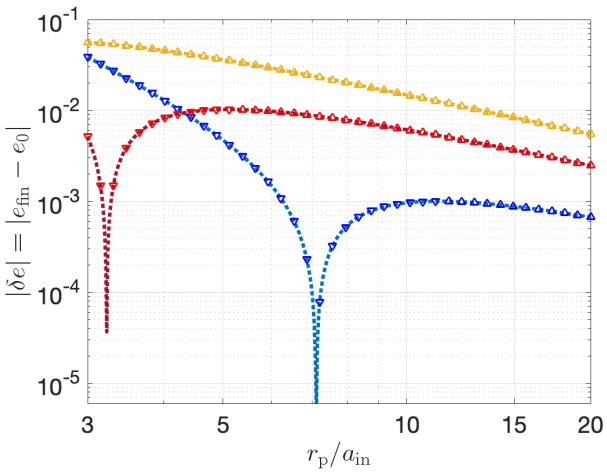

Figure A2. The eccentricity change given by equation (6), for $m_1 = m_2 = m_3 = 20\,M_\odot$, $i_0 = \pi/2$, $\Omega = 0$, $\omega = \pi/4$, and various eccentricities: $e_0 = 0.95$ (yellow), 0.99 (red) and 0.999 (blue). The colours and initial conditions are chosen for comparison with Samsing et al. (2019, figure 4, top panel). Upward-pointing triangles denote $i_\mathrm{final} \leq \pi/2$, while upside-down triangles denote flipped systems, with $i_\mathrm{final} > \pi/2$.

ues, so that the magnitude of the inner orbit's angular momentum decreases. This angular momentum is transferred to the outer orbit, and the naïve map (7) does not readily account for that. To conserve the total angular momentum, we update r_p in each iteration, so that the total angular momentum is conserved. Having modified $\mathbf{j}$ (and thus $\mathbf{J}_\mathrm{out}$, the outer angular momentum), we rotate the frame of reference so that in the next iteration of equation (7), $\mathbf{J}_\mathrm{out} \parallel \hat{\mathbf{z}}$; we update i and Ω accordingly.

APPENDIX B: LONG-TERM EVOLUTION UNDER SECOND-ORDER MAP

In this appendix we discuss several properties of the long-term evolution under the map described in §2. We stress that, as remarked in §4, it is a poor description of isolated quasi-hierarchical triples over time-scales much longer than (a few)$\times\tau_\mathrm{sec}$. However, it may apply qualitatively for triples whose outer orbit can exchange angular momentum with a reservoir. The map itself displays interesting properties, so we keep this discussion here.

Figure B1 shows the value of the orbital parameters after 10000 orbits of the outer binary, as functions of the initial condition $e = e_0$, $i = i_0$ (the angles were randomly selected for each initial condition), for $r_\mathrm{p} = 5a_\mathrm{in}$. We see that given time, more and more initial conditions reach e_u if the initial condition is below i_crit, given by equation (18), and they tend to $e = 0$ and $i = \pi$ if it is above, except for very high initial eccentricities, where the diffusion can nonetheless overcome the negative drift.

B1 First-passage time

For $i_0 \leq i_\mathrm{crit}$, the time to reach e_u (see §4 above) may be obtained from standard first-passage-time calculations, which we describe in appendix C. If the initial values of ω and Ω are selected at random, then the mean time to reach $e = e_\mathrm{max}$ is given by

$$t_\mathrm{max} = T_\mathrm{out}\frac{f(e_0, i_0|e_\mathrm{u})}{\varepsilon^2} \equiv \tau f(e_0, i_0|e_\mathrm{u})\,, \tag{B1}$$

where the diffusion time-scale is defined as $\tau \equiv T_\mathrm{out}/\varepsilon^2$, and f is independent of the semi-major axes and ε, and only depends on the initial condition (e_0, i_0) and on e_u, and satisfies the boundary conditions $f(e_\mathrm{u}, i_0|e_\mathrm{u}) = 0$, $f(0, i_0|e_\mathrm{u}) = \infty$. We plot f and t_max in figure B2 for $i_0 \leq \pi/2 < i_\mathrm{crit}$; f is measured for each pair (e_0, i_0) as the time to reach e_u, where ω_0 and Ω_0 are chosen randomly, evolved using equations (7). f is noisy in the left panel of figure B2, because it measured from one realisation of (ω_0, Ω_0); however, the fact that it is of order unity throughout the parameter space lends credence to the random-walk model. It is evident from the right panel of figure B2, that t_max follows the ε^{-2} scaling predicted by this model to a good accuracy (except possibly at r_p near the limit $\sim 3a_\mathrm{in}$ where the theory breaks down).

Using equations (4) and (B1), the maximum value of r_p for $t_\mathrm{max} \leq t_0$ for some t_0 is therefore

$$r_\mathrm{p,max}^2(t_0) \equiv \min\left\{\left[\frac{t_0}{T_\mathrm{out}}\right]^{\frac{2}{3}} \frac{m_3^{4/3}\,(m_\mathrm{b}M)^{-2/3}\,a_\mathrm{in}^2}{[f(e_0, i_0|e_\mathrm{u})]^{2/3}}, a_\mathrm{in}a_\mathrm{out}\right\}, \tag{B2}$$

where the requirement $r_\mathrm{p,max} \leq \sqrt{a_\mathrm{in}a_\mathrm{out}}$ stems from imposing a *strong* quasi-hierarchical approximation, that is,

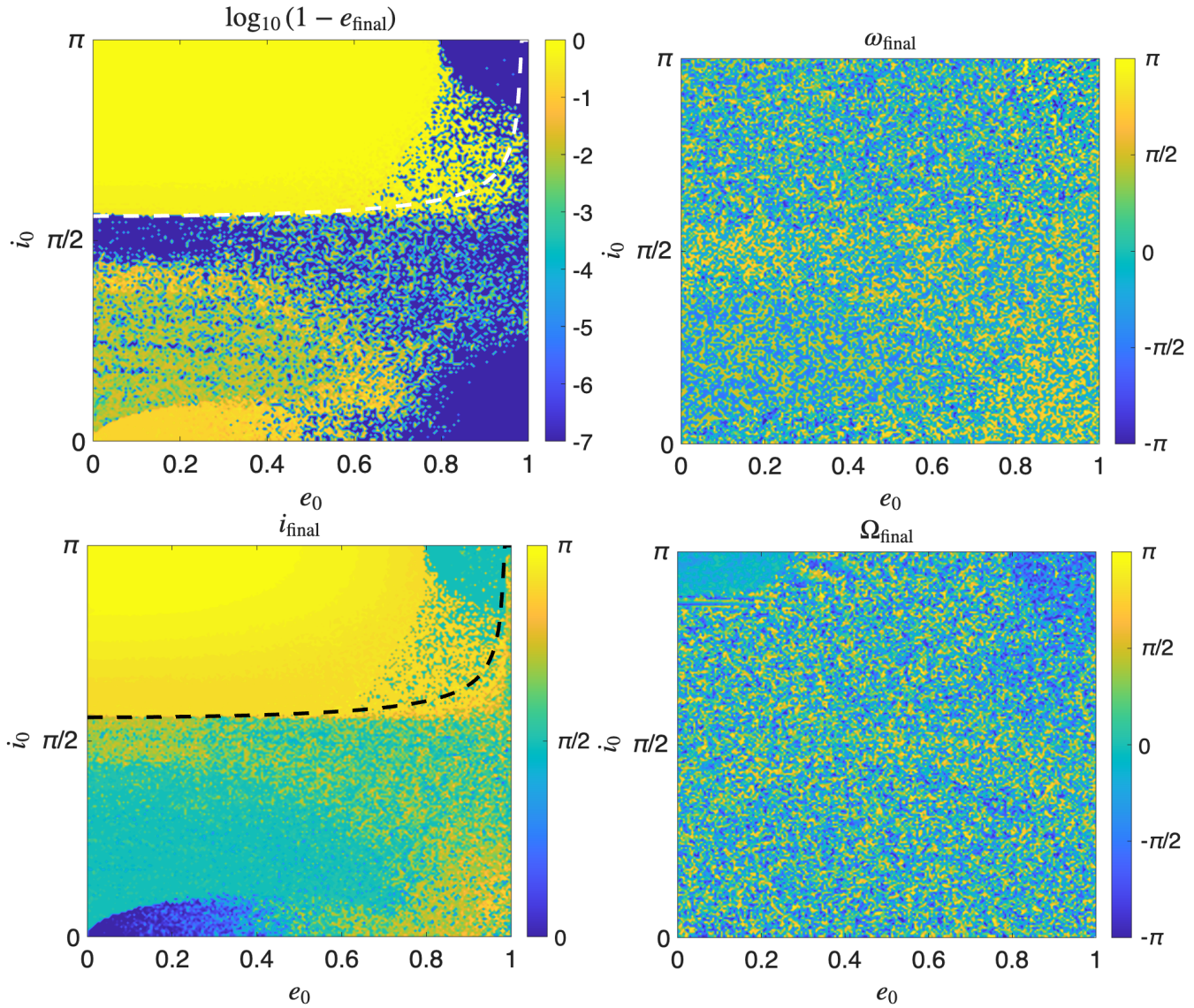

Figure B1. The values of orbital parameters after 10000 outer orbits, for $r_{\rm p} = 5a_{\rm in}$, of randomly chosen initial ω and Ω, as functions of the initial eccentricity e_0 and inclination i_0, for an equal-mass triple. The system is frozen when e_n reaches $1-10^{-7}$. One can see some spin flips in the *bottom left* panel. **e** and **j** are evolved using equations (7), accounting explicitly for angular-momentum conservation. The dashed curve is $i_{\rm crit}$ from equation (18).

that the change in **j** and **e** really be dominated by the pericentre. This is satisfied when $\varepsilon(a_{\rm in}, r_{\rm p}) \geq \varepsilon(r_{\rm p}, a_{\rm out})$, i.e. $r_{\rm p}^2 \leq a_{\rm in}a_{\rm out}$, or, equivalently, $1-e_{\rm out} \leq a_{\rm in}/r_{\rm p}$. Ideally, one would like the inequality to be a strong one, and this is the condition we require here:

$$1-e_{\rm out} \ll \frac{a_{\rm in}}{r_{\rm p}}\,. \tag{B3}$$

B2 Comparison with secular effects

In contrast to secular effects, where the change in orbital parameters is minute over one outer orbit, here Δe and $\Delta\mathbf{j}$ are non-negligible on the time-scale of one outer orbit; so the mechanism described in this paper dominates these time-scales. On longer time-scales, one potentially needs to consider the contributions of the entirety of the outer orbit—not just its pericentre. These are expected to matter over secular time-scales; for a hierarchical triple, the relevant one is the ZLK time-scale, for a corresponding circular outer orbit, given by (Naoz 2016)[6]

$$\tau_{\rm ZLK,circ} = T_{\rm out}\sqrt{\frac{m_{\rm b}M}{m_3^2}\frac{a_{\rm out}^3}{a_{\rm in}^3}}\,. \tag{B4}$$

[6] If we had included the factor of $\left(1-e_{\rm out}^2\right)^{3/2}$ in $\tau_{\rm ZLK}$ in Naoz (2016, equation 27), this would have given $\tau_{\rm ZLK} \sim \tau_{\rm sec} \sim \tau$ by definition. The shortening of the secular time-scale in that case is artificial, because here we wish to compare the effect of the pericentre (encapsulated by τ) to the secular effect of the rest of the outer orbit, *but not including its pericentre* (encapsulated by $\tau_{\rm ZLK,circ}$).

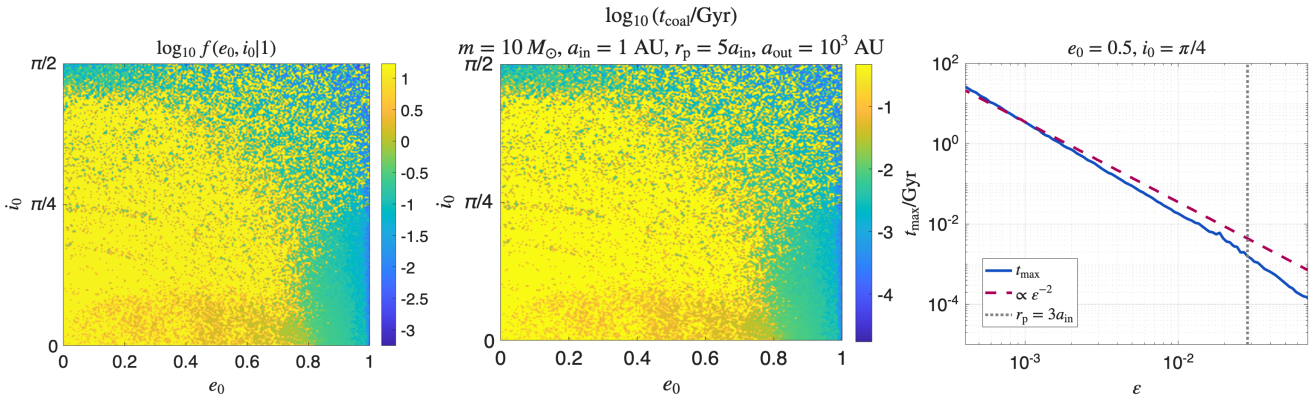

Figure B2. *Left* panel: the function $f(e_0, i_0|1)$, defined in equation (B1). We only show $i_0 \leq \pi/2$ to so that the $i_0 < i_{\rm crit}$ (equation (18)) and a diffusion to $e_{\rm u}$ is ensured. *Middle*: $t_{\rm max}$, measured directly from evolving the triple (as in figure B1), for equal-mass triples with $m = 10\,M_\odot$, $a_{\rm in} = $ AU, $a_{\rm out} = 1000$ AU, $r_{\rm p} = 5a_{\rm in}$. *Right*: $t_{\rm max}$ for an example value of (e_0, i_0) and random ω_0 and Ω_0 (uniform in $[0, 2\pi]$, averaged over multiple draws), for the parameters of the *middle* panel, except $r_{\rm p}$, which is varied.

In contrast, the diffusion time-scale (B1) (which measures the effects of the quasi-hierarchical pericentre 'kicks') is $\tau = T_{\rm out}/\varepsilon^2$. Comparing the two we find

$$\frac{\tau_{\rm ZLK,circ}}{\tau} = \frac{m_3^2}{m_b^{1/2} M^{3/2}} \left(\frac{\sqrt{a_{\rm in} a_{\rm out}}}{r_{\rm p}}\right)^3 = \sqrt{\frac{m_{\rm b}}{M}} \frac{\varepsilon^2}{\alpha^{3/2}}\,, \tag{B5}$$

where $\alpha \equiv a_{\rm in}/a_{\rm out}$; thus, if the quasi-hierarchy is strong enough, τ can be shorter than $\tau_{\rm ZLK,circ}$, and secular effects would be suppressed over the entire diffusion process. The quasi-hierarchical assumption (1) does allow for regimes where this is not necessarily the case, but it is guaranteed by the restriction (B3). To summarise, we have

$$\alpha^{3/4} \left(\frac{m_{\rm b}}{M}\right)^{1/4} \ll \varepsilon \ll 1\,, \tag{B6}$$

to be in the strong quasi-hierarchical regime; and additionally, to reach $e_{\rm u}$ within a time t_0, from equation (B1)

$$\varepsilon \geq \varepsilon_{\rm max}(t_0) \equiv \sqrt{\frac{T_{\rm out} f(e_0, i_0|e_{\rm u})}{t_0}}\,. \tag{B7}$$

B3 Collision Probability

No triple is an island, and the outer tertiary should experience perturbations from its environment, at the same rate that a binary with semi-major axis $a_{\rm out}$ would (Michaely & Perets 2019; Samsing et al. 2019; Michaely & Perets 2020; Grishin & Perets 2022; Stegmann et al. 2024). While Michaely & Perets (2020), for example, consider $e_{\rm out}$ growing to such a high value that $r_{\rm p} \sim a_{\rm in}$ (whereupon a non-hierarchical binary-single encounter ensues), the triple would become quasi-hierarchical, well before reaching that value. At these high eccentricities, we would expect $r_{\rm p}^2$ to be uniformly distributed after the tertiary is perturbed; this implies that it is much more likely that a quasi-hierarchical triple would form, than a fully non-hierarchical one (cf. table 1). If the triple does enter a democratic state, this would eventually result in the ejection or collision of one of the three stars (e.g., Saslaw et al. 1974; Hills 1980; Arnold et al. 2006; Manwadkar et al. 2020; Ginat & Perets 2021), and the eccentricity distribution of the remnant binary after the encounter would be slightly super-thermal (Stone & Leigh 2019; Samsing et al. 2022; Ginat & Perets 2023; Rando Forastier et al. 2025); in the more probable quasi-hierarchical case, the inner orbit can even reach higher eccentricities.

Thus, hierarchical triples are expected to become quasi-hierarchical on the time-scale on which external perturbations would induce an order-unity change in $e_{\rm out}$. The outer orbit may be modified either by encounters from external perturbers, or by the Galactic tide. Fortuitously, the time-scales are quite similar (e.g., Heisler & Tremaine 1986; Binney & Tremaine 2008; Grishin & Perets 2022; Hamilton 2022; Hamilton & Modak 2024), and are collectively given by (Samsing et al. 2019)

$$\tau_{\rm ext} = \frac{1}{2\pi G} \frac{\sigma}{\rho a_{\rm out}} \frac{m_*}{(M + m_*)}, \tag{B8}$$

where m_* is the average stellar mass of the triple's environment. We remark that $\tau_{\rm ext}$ is typically significantly longer than τ; this can be seen in figure B2, which shows that $\tau \ll$ Gyr, while $\tau_{\rm ext} \sim$ Gyr.

Let us, therefore, assume that $e_{\rm out}$ is thermally distributed. Then, the probability for the inner binary reaching $e_{\rm u}$ within a time t_0 is equal to the probability that $r_{\rm p} \leq r_{\rm p,max}(t_0)$, i.e.

$$P(t_0|a_{\rm in}, a_{\rm out}, e_0, i_0) = 1 - \left[1 - \frac{r_{\rm p,max}(t_0)}{a_{\rm out}}\right]^2 \approx 2\frac{r_{\rm p,max}(t_0)}{a_{\rm out}}\,. \tag{B9}$$

This probability corresponds to stating that the outer eccentricity $e_{\rm out}$ is constantly excited to values which are thermally distributed by the environment, on a time-scale $\tau_{\rm ext}$.

Given a model for hierarchical triples—for e_0,i_0, $a_{\rm out}$—one can use equation (B9) to derive a probability $P(t_0|a_{\rm in})$ for reaching $e_{\rm u}$ within a time t_0. Furthermore, if $e_{\rm u}$ and t_0 are chosen such that the diffusion time plus the time-to-coalescence is less than the typical time between encounters with the outer body, one can finally find a probability of merging as a function of $a_{\rm in}$ and the masses, only.

B4 Eccentricity boundary

We determine $e_{\rm u}$ by requiring two separate criteria, which we described in the following two sub-sections.

B4.1 Maximum eccentricity reachable by random walk

The random walk may only drive e efficiently until a certain value of e, above which most values of ω (and the other angles) would yield $\Delta e < 0$ (cf. figure A1). Again, assuming $i \approx \pi/2$, we find that if $1 - e \ll 1$,

$$\Delta e \simeq \frac{15\pi}{4}\varepsilon\sqrt{1-e^2}\sin 2\omega + \frac{225}{64}\left(\pi^2\varepsilon^2\cos 4\omega - \pi^2\varepsilon^2\right) \ ; \tag{B10}$$

for $\Delta e \geq 0$, one must have

$$\sqrt{1-e_{\rm u}^2} \geq \frac{15\pi}{8}\varepsilon\sin 2\omega. \tag{B11}$$

Squaring and averaging this over ω one finds

$$1 - e_{\rm u}^2 \geq \frac{225\pi^2}{128}\varepsilon. \tag{B12}$$

B4.2 Beyond-Newtonian point-particle effects

A cut-off for $e_{\rm u}$ can also be derived by requiring that it not be sufficiently high, that the orbital parameters of the inner binary would evolve significantly over one outer orbit, e.g. due to gravitational-wave emission, tidal effects, *etc.* (any additional mechanism for angular-momentum evolution would do). This is essentially equivalent to demanding that the eccentricity change over one outer orbit be of the same order of magnitude as that due to gravitational wave, that is

$$\frac{1}{T_{\rm out}}\sqrt{\langle\Delta e^2\rangle} \sim \left(\frac{{\rm d}e}{{\rm d}t}\right)_{\rm ext}, \tag{B13}$$

where both sides are evaluated at $e = e_{\rm u}$, and it is assumed that by then $i \approx \pi/2$. Here, $({\rm d}e/{\rm d}t)_{\rm ext}$ is the eccentricity change due to the additional physical mechanism; henceforth we take this to be gravitational-wave emission as an illustrative example, whence in that case

$$1 - e_{\rm u,gw}^2 \geq \left(\frac{68\sqrt{2}T_{\rm out}}{477\pi\varepsilon\tau_{\rm c}}\right)^{1/3}, \tag{B14}$$

where $\tau_{\rm c}$ is the time-to-coalescence of a binary, given by

$$\tau_{\rm c} = \frac{5}{256}\frac{c^5 a_{\rm in}^4}{G m_{\rm c}^{5/3} m_{\rm b}^{4/3}}, \tag{B15}$$

where $m_{\rm c}$ is the inner binary's chirp mass.

$e_{\rm u}$ obtained this way is very close to 1; and we combine this with the requirement in inequality (B12). Together

$$e_{\rm u,gw}^2 = 1 - \max\left\{\frac{225\pi^2}{128}\varepsilon, \left(\frac{68\sqrt{2}T_{\rm out}}{477\pi\varepsilon\tau_{\rm c}}\right)^{1/3}\right\}, \tag{B16}$$

where it is understood that $e_{\rm u} \equiv 0$ if the right-hand side evaluates to a negative number.

APPENDIX C: FIRST-PASSAGE TIME

As discussed in §4, the long-term evolution under equations (5) and (7) suggests that e and i evolve as a random walk, where ω and Ω are essentially viewed as randomised in each step. The continuum limit of this system (where $\varepsilon \to 0$ and the number of steps tends to infinity) is a Fokker–Planck equation, of the form

$$\frac{\partial p}{\partial t} = \frac{\partial}{\partial x^k}\left[D_2^{jk}(e,i)\frac{\partial p}{\partial x^j}\right] + \beta(e,i)\frac{\partial}{\partial x^k}\left[D_1^k(e,i)p\right] \equiv \mathcal{D}[p] \ , \tag{C1}$$

where $x^j \equiv (e,i)$ is a two-dimensional shorthand, and the diffusion coefficients are $D_1^k, D_2^{jk} = \mathcal{O}(\varepsilon^2)$, because the drift $\langle\Delta e\rangle$ vanishes at first order in ε. The initial condition is

$$p(e,i,t=0) = \delta^{\rm D}(e-e_0)\delta^{\rm D}(i-i_0) \ , \tag{C2}$$

where $\delta^{\rm D}$ is Dirac's delta-function.

For such a process the mean first-passage time, defined as the mean time for a walker to reach $e = e_{\rm u}$, starting at $x_0 = (e_0, i_0)$, is necessarily (Redner 2001)

$$t_{\rm max}(x_0|e_{\rm u}) \propto \frac{1}{\varepsilon^2} \ . \tag{C3}$$

This may be seen from the associated continuum problem (C1), where $t_{\rm max}$ satisfies a backward Kolmogorov equation (Redner 2001)

$$\mathcal{D}^\dagger\left[t_{\rm max}\right] = -1, \tag{C4}$$

with a boundary condition $t_{\rm max}(e_{\rm u}, i_0|e_{\rm u}) = 0$. The adjoint Fokker–Planck operator is

$$\mathcal{D}^\dagger[t] = \frac{\partial}{\partial x_0^k}\left[D^{jk}(e_0,i_0)\frac{\partial t}{\partial x_0^j}\right] - \beta(e_0,i_0)D_1^k(e_0,i_0)\frac{\partial t}{\partial x_0^k} \ , \tag{C5}$$

and is therefore $\mathcal{D}^\dagger \propto \varepsilon^2$; that is, re-scaling the unit of time $T_{\rm out}$ and ε^2 are interchangeable. This yields equation (B1).

This paper has been typeset from a TEX/LATEX file prepared by the author.